

Microfacet Scattering Model for Pulse Polarization Ranging

Dr. John Stryjewski

Dan Hand,
CSC-ISTEF

Dr. David Tyler

Sukumar Murali

College of Optics, University of Arizona

Dr. Mike Roggemann

Nick Peterson

Department of Electric and Computer Engineering

Michigan Technological University

09/1/2009

Abstract

Determining the shape, material and orientation of nano-sats (satellites too small to image from the ground) requires new sensing approaches. Pulse Polarization Ranging (PPR) is one such approach that uses the polarization and shape characteristics of laser pulses reflected from satellites to determine satellite shape, orientation and material. We use an innovative approach to relate PPR measurements to actual satellite characteristics (shape, material and orientation), which requires that we have an accurate physical and dynamical model of the satellite. In particular, to determine the polarization characteristics (depolarization, birefringence, diattenuation) of the reflected pulses we need an accurate model of light scattering from real (complex) surfaces. To do this, we have extended the micro-facet model of Ashikhmin et al to include retro-reflection and multiple scattering effects. In this presentation, we describe the scattering model and its efficient implementation using graphical processing units (GPUs).

Introduction

When a satellite is large or in low earth orbit, imaging systems can be used to determine its shape and orientation. With an imaging spectrometer it may be possible to identify the material present in the satellite. However, with the advent of modern construction and packaging technologies satellites are becoming smaller and smaller. It is already possible to build satellites that even a 6m aperture can not resolve in Low Earth Orbit (LEO). For satellites in high orbits, the problem is even harder.

How does one determine the shape, orientation and material composition of an unresolved object in LEO? Clearly, one could use a spectrometer to analyze the light reflecting off of the satellite and determine its material composition. However, with such small objects there may not be enough light for spectroscopy. The time evolution of the intensity of reflected sunlight is sensitive to the orientation of the satellite but, this is only useful during daytime. One could also use synthetic aperture approaches to image the satellite and determine its shape and orientation.

Methods that rely on the intensity of reflected light have two potential difficulties. First, only sunlit satellites can be examined unless laser illumination is used. Second, any intensity based approach, such as spectroscopy or time evolution of reflected light intensity, must deal with atmospheric and cloud extinction. This is irrespective of whether natural or artificial illumination is used. In practice the uncertainty in the extinction

is the biggest source of error in intensity based approaches. One solution is to use Doppler (coherent) approaches where frequency shifts and not absolute intensity are important. However, while Doppler methods are well suited for shape and orientation determination, they are not well suited for determining material composition.

Our goal was to devise an approach that was not affected by atmospheric extinction and could estimate the shape, orientation and material of an unresolved satellite in LEO. This meant that intensity-based and spectroscopic approaches were not acceptable. Coherent approaches such as Range-Doppler imaging and Synthetic Aperture have been well studied elsewhere and we felt that a new approach was necessary.

We chose to consider only approaches where the satellite is actively illuminated because they allow observation during day or night. The technique we chose was Pulse Polarization Ranging (PPR). In PPR, a very short pulse, typically 100ps in duration, is reflected off an object and two effects are measured: the stretching of the pulse due to the range depth profile of the object and the polarization signature of the object. All polarization effects are range resolved so we have a detailed 1D polarization-shape profile of the object. Intensity calibration of the return pulses is not necessary since both the shape and polarization information is unaffected by atmospheric extinction, greatly simplifying the data analysis.

The critical part of the procedure is to successfully invert the 1D shape-polarization profiles to estimate the shape, orientation and materials of the object. Numerous studies over the past 10-15 years have shown that the 1D shape profile can be used to estimate orientation or pose of a known object and to a lesser extent the pose and shape of an unknown object. Also, a number of studies[1] have shown that polarization signatures of unresolved objects can be used to determine basically any two properties (material, shape and orientation) if one is known. Our approach combines the strength of both the pulse profile and polarization approaches, thus maximizing the information about the target.

Critical to making the PPR approach viable is good inversion technique to go from depth only shape and polarization data to shape, orientation, and material properties of the target. The method we use is based on a vector classifier approach where the data is represented as a vector in some multi-dimensional vector space. The inversion is accomplished by comparing this data vector to possible candidate objects using a weighted inner product. This weighting may be chosen to best recover any combination of shape, orientation, material or finish.

To make this vector classifier viable we must have a way of constructing a database of candidate objects with different shapes, orientations, materials and finishes. Constructing such databases from experimentally measured objects is certainly possible however, it would be very expensive and would not provide us with the ability to *predict* new signatures. Additionally, storing the polarization properties of objects is prohibitively expensive as we will see in the next section. Finally, relying only on experimental data gives us limited insight into the underlying physics and thus a limited understanding of what information is most important for discriminating object properties.

Therefore, we have chosen to develop a first-principle model of PPR that accurately models shape, orientation and material properties of objects. This model not only allows us to investigate the basic physics of the PPR process but it also provides a compression algorithm for generating our object database. This model is based on cutting edge techniques used in the motion picture and computer gaming industries for computer animation and scene generation. Our approach makes use of advanced in computational image generation methods and hardware acceleration to greatly increase the speed of calculations. In this paper we will explain these techniques and describe how we extended them in a way that handles PPR in a physically rigorous and computationally tractable manner.

Polarization Signatures

Consider the light scattering from a surface (Figure 1). Scattering from a surface may be described by the Bidirectional Reflectance Distribution Function or BRDF.

$$f(k, k') = \frac{dL}{dI} \quad (1)$$

Where dI is the irradiance incident on the surface and dL is reflected radiance. Equation 1 for the BRDF is valid for unpolarized light only and is a function of 4 variables, two input and two output angles. This function can be determined experimentally and stored as a lookup table or fitted to a special function. This provides a convenient way to describe surface scattering in the case of unpolarized light. However, if the surface exhibits polarization effects then the reflection is described by a Mueller matrix2:

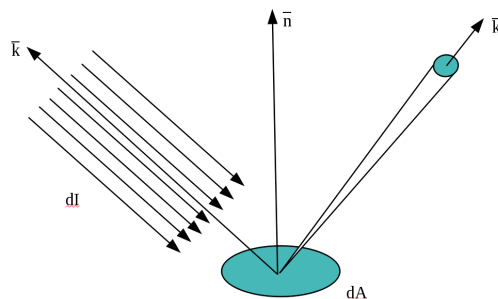


Figure 1: BRDF Geometry

When the surface exhibits polarization effects then the reflection is described by a Mueller matrix2:

$$\begin{bmatrix} S'_0 \\ S'_1 \\ S'_2 \\ S'_3 \end{bmatrix} = \begin{bmatrix} M_{00} & M_{01} & M_{02} & M_{03} \\ M_{10} & M_{11} & M_{12} & M_{13} \\ M_{20} & M_{21} & M_{22} & M_{23} \\ M_{30} & M_{31} & M_{32} & M_{33} \end{bmatrix} \cdot \begin{bmatrix} S_0 \\ S_1 \\ S_2 \\ S_3 \end{bmatrix} \quad (2)$$

Where S is the Stokes vector which describes the polarization state of the light. The Mueller matrix describes the change in polarization when light reflects from a uniform, flat surface. This means that our 4 dimensional BRDF is now a 20 dimensional BRDF. Actually, in practice, not all degrees of freedom are independent and generally less than 12 elements are independent, depending on symmetries. For curved, textured or multi-layered surfaces the problem can be prohibitively complicated to store sufficient data to characterize an object. So rather than rely solely on measured data, we decided to derive a first principles theory of surface scattering that is validated with experimental data when possible.

Microfacet Model

The requirements for our model are: that it be radiometrically accurate, conserve energy, exhibit Helmholtz reciprocity and be numerically tractable. This last point is very important since we will be using the model to generate as many object realizations as possible to improve the performance of our inversion algorithm.

Figure 2 shows examples of measured and computer generated images of satin tape wrapped around a spindle. The computer generated image is practically indistinguishable from the real image. This is no accident, the method used to generate the image on the right is physics based and radiometrically accurate.

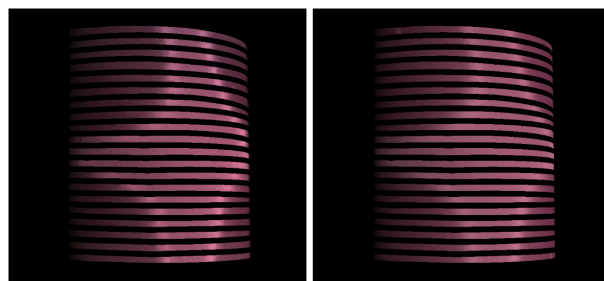


Figure 2: Left: Real image of purple satin, Right: Computer generated image[1]

Figure 3 shows another image of a computer generated satin draped over a table. The subtle change in hue with angle that is characteristic of satin is even

reproduced. The images in Figures 2-3 were generated from first principles using a Micro-Facet (MF) model of light scattering. The lighting and overall geometry were modeled using standard computer graphics methods.

The MF approach grew out of a desire by the computer gaming and movie animators for more realistic scene generation. In this approach, effects due to the surface structure on scales smaller than a wavelength can be ignored. This assumption has been shown by rigorous calculations to be appropriate[8] since, any diffraction effects will average out at normal viewing distances. Surface geometry at scales much greater than the surface roughness correlation distance are modeled explicitly using standard 3-D modeling methods such as: polygonal facets, geometric primitives or Bezier splines. The meso-scale, between the microscopic diffraction scale and the explicitly described macro scale, included all of the “surface roughness” scales and are modeled statistically. In this approach the surface is modeled as an ensemble of microfacets (figure4). These facets need not be planar; they can have any number of geometric and physical properties. However, Ashikhmin[12] and He[8] have shown that triangular, plainer facets are sufficient to describe any surface; in fact, all of the facets can be identical. In the case of identical, planar microfacets, only three parameters are necessary to fully describe the surface micro-structure: the distribution of surface normal directions, the surface roughness and the index of refraction.



Figure 3: Rendering of velvet

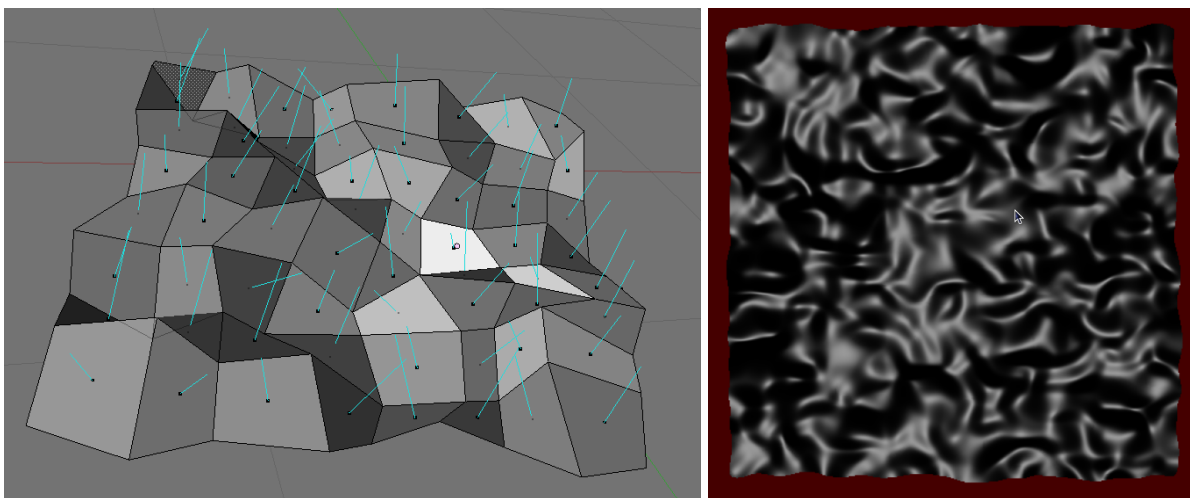


Figure 4: Left: microfacet surface, blue arrows are normals. Right: fractal surface with 130k facets

We have chosen to use a the Blinn-Phong normal distribution to describe the microfacet normal distribution

$$\rho(h) = \left(\frac{m+1}{2\pi} \right) \cos(\hat{h} \cdot \hat{n})^m \quad (3)$$

Here, \hat{h} is the microfacet normal, \hat{n} is the local average (macro-scale) surface normal and m is a surface roughness parameter proportional to the inverse of the surface correlation distance. A Lambertian surface would have $m = 0$ and a mirror surface would have $m = \infty$. This distribution has a number of computational advantages and, more importantly, it has been experimentally justified[11] for a number of materials. While the results presented here use the Blinn-Phong normal, there are no a priori restrictions on the distribution, it is not even required to be analytic.

One of the key features of the microfacet theory is the concepts of shadowing and masking (Figure 5). If under illumination a microfacet is shadowed by another microfacet it does not contribute to the BRDF. Likewise if a microfacet is not visible to the “viewer” then it is said to be masked, and does not contribute to the BRDF. Since, the BRDF is symmetric with respect to interchange of k and k' we will henceforth refer to both effects as shadowing. Thus, the microfacet BRDF can be written as:

$$f(\hat{k}; \hat{k}') = \left(\frac{\rho(\hat{h})}{\langle \hat{n} \cdot \hat{h} \rangle (\hat{n} \cdot \hat{k})} \right) F(\hat{k}, \hat{k}') P(\hat{k}|\hat{k}') \quad (4)$$

Here the factor $P(k|k')$ is the probability that a microfacet is visible from both the k and k' directions and contains the shadowing effects. The term $F(k|k')$ is the Fresnel reflection term which contains the surface physics. Ashikhmin used the unpolarized (average) Fresnel approximation of Shick[6]:

$$F(k; k') = F_0 + (1 - F_0) \left(1 - (\hat{h} \cdot \hat{k}) \right) \quad (5)$$

Here \hat{h} is the half-angle vector between k and k' , which is just the microfacet normal, and F_0 is the normal incident angle. The term $\langle \hat{n} \cdot \hat{h} \rangle$ in Equation 4 is the ensemble average over the distribution $\rho(\hat{h})$.

Ashikhmin et al. have shown that the general form of the shadowing term, $P(k|k')$ in Equation 4 is:

$$P(k|k') = (1 - f(\phi)) P(k)P(k') + f(\phi) \min(P(k), P(k')) \quad (6)$$

where $f(\phi)$ is a function of the angle, ϕ , which is the angle between the projections k and k' onto the plane normal to \hat{n} , the surface normal. For our work we choose the simplest form for $f(\phi)$ which is consistent with Equation 6 namely, $f(\phi) = \cos(\phi/2)$. Finally, the function $P(k)$ is the probability that a microfacet is visible from the direction k :

$$P(k) = \frac{\langle \hat{n} \cdot \hat{h} \rangle (\hat{n} \cdot \hat{k})}{\langle \hat{h} \cdot \hat{k} \rangle_+} \quad (7)$$

Here the ensemble average, $\langle \hat{h} \cdot \hat{k} \rangle_+$, is over all microfacets that are not shadowed (or masked). For details on the derivation refer to Ashikhmin’s paper[2]. The important point here is that once the microfacet normal distribution is specified, the BRDF is specified. Also note that this BRDF only contains contributions from single bounce (specular) reflections, To account for multiple reflections, Ashikhmin et al enforced energy conservations and reciprocity to derive a unique expression for the multiple reflection (diffuse) reflection term.

$$f_d = c(1 - R(k))(1 - R(k')) \quad (8)$$

Here the function $R(k)$ is the total hemispherical specular reflectance for light incident from direction k . The total BRDF is then the sum of a specular (single reflection) and a diffuse (multiple reflection) BRDF:

$$f = f_{specular} + f_{diffuse} \quad (9)$$

The optical effects that this simple, physics based approach is capable of reproducing is quite striking (Figures 2,3). For laser *backscatter* the specular term in Equation 9 is polarization preserving since all

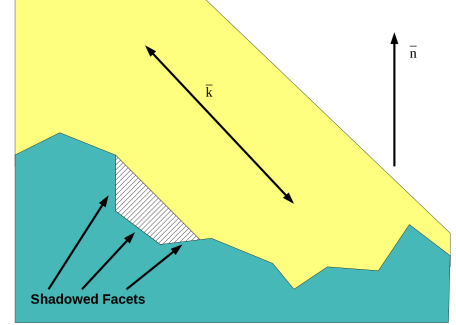


Figure 5: Shadowing and Masking

reflections are normal to the microfacet surfaces. In general, multiple reflections depolarize, and the diffuse term gives the depolarization. Thus, if depolarization is the only polarimetric quantity of interest this formulation is a good approximation. Though not shown here, the Ashikhmin-Shirley approach can also represent simple surface roughness anisotropy by introducing an anisotropic $\rho(h)$ [12] (see Figure 6).

However, if we want to model the other polarimetric quantities such as retardance and diattenuation a more sophisticated approach is warranted. In the following sections we derive extensions to the Ashikhmin-Shirley approach that explicitly handle double reflections and a polarization effects in a rigorous manner.

Polarization

To handle general polarization effects in a rigorous manner is simply a matter of replacing the unpolarized Fresnel term of Shick[6] with the full Fresnel representations for the s and p polarizations:

$$r_s = \frac{\sqrt{n^2 - \sin(\theta)^2} - \cos(\theta)}{\sqrt{n^2 - \sin(\theta)^2} + \cos(\theta)} \quad (10)$$

$$r_p = \frac{n^2 \cos(\theta) - \sqrt{n^2 - \sin(\theta)^2}}{n^2 \cos(\theta) + \sqrt{n^2 - \sin(\theta)^2}} \quad (11)$$

Here n is the index of refraction of the material (in air) and $\cos(\theta)$ is the angle of reflection with respect to the *microfacet* normal. Note, that the above Fresnel equations, *for the reflection field amplitudes*, are valid for complex n and thus can be used with metals or dielectrics. By adding the polarization in this way we can now calculate polarimetric quantities such as: retardance, diattenuation and depolarization.

Double Reflection

Adding the full Fresnel term to the Ashikhmin MF model will give very good polarization results for situations where the illumination and the observer are separated by greater than about 5 degrees. For rough surfaces at illumination-observer angles less than about 5 degrees double reflections contribute significantly to the polarization signature of object.

Figure 7 shows the double reflection geometry for 180° backscatter. Note that the scattering plane for the first and second reflections are the same, leading to strong polarization effects. As the illumination-observer



Figure 6: Anisotropic silk, from Kautz et al[4]

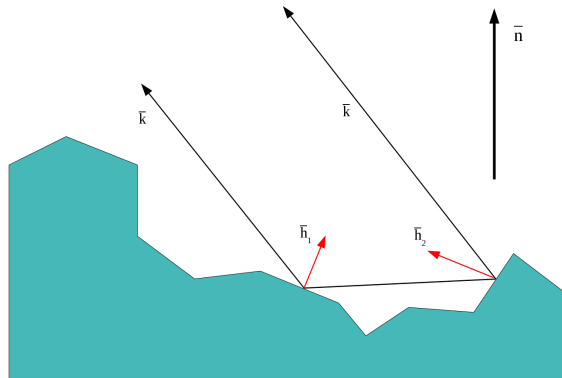


Figure 7: Double bound backscatter geometry

separation increases these correlations decrease and the polarization effects fade. Also, since the optical path for the retro reflection is reciprocal, the forward and reverse reflections will add coherently. This is the famous enhanced backscatter effect and results in a factor 2 enhancement of for double scattering.

In our model we extend the work of Ashikhmin and others by adding rigorous polarization and double reflection expressions. Also, we use field amplitudes as opposed to intensities, this allows us to easily handle coherent effects such as enhanced backscatter. In this new model the total BRDF is

$$f = f_{single} + f_{double} + f_{multiple} \quad (12)$$

where f_{single} is a single bounce specular term, $f_{multiple}$ is Ashikhmin's multiple scattering term modified to remove double reflection effects and f_{double} is our double reflection extension;

$$f(\hat{k}; \hat{k}')_{double} = \left(\frac{1}{\langle \hat{n} \cdot \hat{h} \rangle (\hat{n} \cdot \hat{k})} \right) \langle \rho(\hat{h}) F_2(\hat{k}, \hat{k}') P_2(\hat{k} | \hat{k}') \rangle \quad (13)$$

Here the ensemble average is over all possible combinations of h_1 and h_2 (see Figure 7) that contribute to a double reflection from k to k' . For the special case of 180 degree backscatter h_1 and h_2 are related since,

$$(h_1 \cdot h_2) = 0 \quad (14)$$

The function F_2 is the combined Fresnel reflection coefficient for the double bounce. In terms of the field amplitudes for s and p polarizations they are

$$r_{s2} = \left(\frac{\sqrt{n^2 - (\hat{k} \cdot \hat{h}_2)^2} - (\hat{k} \cdot \hat{h}_1)}{\sqrt{n^2 - (\hat{k} \cdot \hat{h}_2)^2} + (\hat{k} \cdot \hat{h}_1)} \right) \left(\frac{\sqrt{n^2 - (\hat{k} \cdot \hat{h}_1)^2} - (\hat{k} \cdot \hat{h}_2)}{\sqrt{n^2 - (\hat{k} \cdot \hat{h}_1)^2} + (\hat{k} \cdot \hat{h}_2)} \right) \quad (15)$$

$$r_{p2} = \left(\frac{n^2 (\hat{k} \cdot \hat{h}_1) - \sqrt{n^2 - (\hat{k} \cdot \hat{h}_2)^2}}{n^2 (\hat{k} \cdot \hat{h}_1) + \sqrt{n^2 - (\hat{k} \cdot \hat{h}_2)^2}} \right) \left(\frac{n^2 (\hat{k} \cdot \hat{h}_2) - \sqrt{n^2 - (\hat{k} \cdot \hat{h}_1)^2}}{n^2 (\hat{k} \cdot \hat{h}_2) + \sqrt{n^2 - (\hat{k} \cdot \hat{h}_1)^2}} \right) \quad (16)$$

The double bounce probability $P_2(k|k')$ in the ensemble average is the probability of a specific double bounce, defined by h_1 . It is given by

$$P_2(k|k') = \frac{(P_1(k) - P_1(k|k')) (P_1(k) - P_1(k|-k'))}{(1 - P_1(k|-k'))} \quad (17)$$

Here, k' is the direction from surface 1 to surface 2; $P_1(k)$ and $P_1(k|k')$ are the single bounce visibility probabilities, Equations 7 and 6.

Because the terms P_2 and F_2 in the ensemble average (Equation 13) depend on the microfacet normals h_1 and h_2 , the average must be evaluated numerically. And, since we want to compute polarization effects on laser backscatter from complicated objects (satellites) and our PPR inversion technique requires many solutions model realizations, we need an efficient way of computing $f(k|k')_{double}$.

Computer Implementation

Our computer implementation draws upon the experience of the real-time computer gaming industry, namely the use of specialized graphics hardware. Until recently, complicated illumination calculations like ours would require hours on a computer using ray-tracing techniques (citation). However, recent hardware implementations using Graphical Processing Units (GPUs) such as NVIDIA™8000 and 9000 series graphics boards has made it possible to render (generate) thousands of full 3D realizations per second. This hardware is available for only a few hundred dollars and is available for almost all computing platforms. In addition to the NVIDIA™GPU hardware, we make use of a number of software programming tools including: OpenGL, a 3D graphics package; GLSL, the OpenGL Shader Programming Language and CUDA, NVIDIA’s general purpose computing language for GPUs.

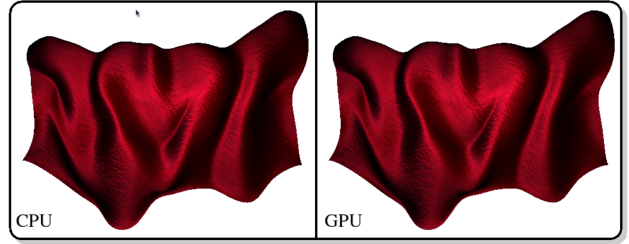


Figure 8: Left: ray traced image; Right, shader generated (from [4])

One of the choices we made was to use a shader based rendering approach rather than a ray tracing approach. The details of this trade-off are beyond the scope of this paper. While ray tracing is a more general approach, for most applications, the shader approach is best because of the tremendous increase in speed. Figure 8 shows some results from Kautz[4] et al that compare the ray tracing to the shader approach for rendering cloth using BRDFs.

Our approach requires a number of ensemble averages to be calculated; the first of these is:

$$\langle (\hat{k} \cdot \hat{h}) \rangle_{+} = \frac{m+1}{\pi} \iint_{(\hat{k} \cdot \hat{h}) > 0} (\hat{k} \cdot \hat{h}) \sin(\theta)^{m+1} \cos(\phi)^m d\theta d\phi \quad (18)$$

This integral can be solved with a series expansion for $\int \cos(\theta)^m d\theta$, however, the series does not evaluate well numerically because it contains ratios of factorials. In fact, even with double precision, the standard solution becomes unstable for $m > 5000$, which corresponds to smooth surfaces. Because of this instability and the need for a very efficient solution, we derived an analytic approximation to $\int \cos(\theta)^m d\theta$ namely;

$$\int_{\alpha}^{\frac{\pi}{2}} \cos(\theta)^m d\theta \cong 2A(m) - A(m) (1 - A(m) \cos(\alpha))^{m+1} \quad (19)$$

where,

$$A(m) = \frac{\pi}{2} \frac{m!}{2^m (\frac{m}{2}!)^2} \quad (20)$$

Here we still have the problem of evaluating an expression with large $m!$. To solve this we derived an expression for $m!$ which is exact for $m = 0$ and approaches Sterling approximation for large m :

$$m! \cong \sqrt{2\pi m + 1} e^{-m} m^m \quad (21)$$

using this approximation we find that:

$$A(m) \cong \frac{\pi}{2} \frac{\sqrt{2\pi m + 1}}{n\pi + 1} \quad (22)$$

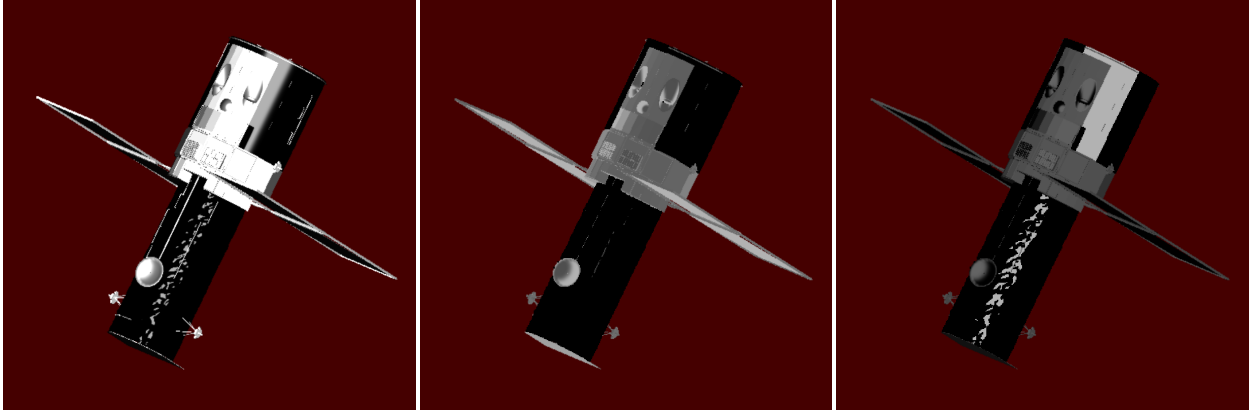


Figure 9: Simulated image of Hubble Space Telescope: left image is the total reflectance, middle image is depolarization and right image is polarizance

Using (19) and (22) we find that:

$$\langle \hat{k} \cdot \hat{h} \rangle_{+=} = \frac{m+1}{\pi} \cos(\alpha) \left[2A(m+1) - A(m+1)\cos(\alpha)^{m+2} + \tan(\alpha) \frac{\sin(\alpha)^{m+1}}{m+1} \right] \cdot A(m+2) \quad (23)$$

Having this closed form expression for $\langle \hat{k} \cdot \hat{h} \rangle_{+=}$ allows us to evaluate f_{double} for $0 \geq m > 10^6$, making it possible to handle diffuse and specular surfaces with the same model.

Figure 9 shows some preliminary results from our model. The materials shown are not the actual HST materials, they are generic and intended only for illustration purposes. The left hand image is the total reflectance for 180 degree backscattered laser light, the middle image is the percent polarization preserving (the polarizance) and the right hand image is the depolarization ratio. These results are preliminary and some computer implementation (coding) work remains to extract diattenuation and retardance. However, all of the parts of the model are in place to produce high fidelity polarization images of realistic satellites and PPR shape-polarization profiles. Note: the wrinkled thermal wrap on the telescope tube.

Summary

We have developed polarization and double reflection extensions to the Ashikhmin's microfacet scattering theory. These extensions are physically based and yield BRDFs that conserve energy and Helmholtz reciprocity. This approach allows us to accurately describe the physics of laser backscatter from complicated objects. This includes effects such as shape, orientation, material and surface finish. Additionally, our GPU based approach allows us to easily include the effects of solar illumination and thermal emission, atmospheric effects (turbulence and transmission) and satellite dynamics. Additionally, our approach calculates the electric field, as opposed to the intensity, so coherent effects such as enhanced backscatter are included naturally.

The microfacet approach is very general and can be easily extended to handle multilayer surfaces, emission, and refraction and transmission. Even complicated, textured material like cloth, scratched metal and wood are readily modeled. With minor modifications our approach can also handle reflections from liquids, gasses and particulates[1, 5].

This work was funded significantly by AFOSR grant FA9550-07-1-035B

References

- [1] Gerligand, P., Smith, M., Chipman, R. *Polarimetric Images of a Cone*, Optics Express, vol. 4, No 10, 420-430, 1991
- [2] Ashikhmin, M., Premoze, S., Shirley, P., *A Microfacet-based BRDF Generator*, SIGGRAPH, 65-74, 2000
- [3] Walter et al, *Microfacet Models for Refraction through Rough Surfaces*, Eurographics Symposium on Rendering, 2007
- [4] Kautz, Jan et al, *User Defined Shading Models for VR Applications*, 2005
- [5] Cook R. and Torrence K., *A Reflection Model for Computer Graphics*, SIGGRAPH, 192-198, 1981
- [6] Shick, C., *An Inexpensive BRDF Model for Physically based Rendering*, Eurographics, 149-162, 1994
- [7] Ward., *Measuring and Modeling Anisotropic Reflection*, SIGGRAPH, 265-272, 1992
- [8] He. X.D. et al, *Comprehensive Model for Light Reflection*, SIGGRAPH, 176-186, 1991
- [9] Torrence, K.E. and Sparrow, E.M., *Theory of Off-specular Reflection from Rough Surfaces*, JOSA, 57, 1957
- [10] Weidlich, A. and Wilkie, A., *Arbitrarily layered micro-facet surfaces*, 2006
- [11] Ngan, A et al, *Experimental Analysis of BRDF Models*, Eurographics Symposium on Rendering, 2005
- [12] Ashikhmin, M. and Shirley, P., *An Anisotropic Phong light Reflection Model*, *Journal of Graphics Tools*, 25-32, 2000